Influence of Zn Interlayer on Interfacial Microstructure and Mechanical Properties of TIG Lap-Welded Mg/Al Joints

Qiong Gao and Kehong Wang

This study explored 6061 Al alloy and AZ31B Mg alloy joined by TIG lap welding with Zn foils of varying thicknesses, with the additional Zn element being imported into the fusion zone to alloy the weld seam. The microstructures and chemical composition in the fusion zone near the Mg substrate were examined by SEM and EDS, and tensile shear strength tests were conducted to investigate the mechanical properties of the Al/Mg joints, as well as the fracture surfaces, and phase compositions. The results revealed that the introduction of an appropriate amount of Zn transition layer improves the microstructure of Mg/Al joints and effectively reduces the formation of Mg-Al intermetallic compounds (IMCs). The most common IMCs in the fusion zone near the Mg substrate were Mg-Zn and Mg-Al-Zn IMCs. The type and distribution of IMCs generated in the weld zone differed according to Zn additions; Zn interlayer thickness of 0.4 mm improved the sample's mechanical properties considerably compared to thicknesses of less than 0.4 mm; however, any further increase in Zn interlayer thickness of above 0.4 mm caused mechanical properties to deteriorate.

1. Introduction

Problems related to climate change and resource scarcity continue to grow more severe. Within the aerospace industry, the response to global warming has included efforts to reduce the weight of aerospace structures and vehicle bodies via lightweight materials that reduce fuel consumption and ease pressure on the fuel economy. To this effect, magnesium (Mg) and aluminum (Al) alloy materials have garnered the interest of researchers and developers in not only the aerospace community, but also in automotive, electrical, and chemical fields; these materials are favored in view of their outstanding performance, low density, and light weight. Successfully and efficiently joining Mg and Al alloys affords manufacturing flexibility and design freedom, which are necessary for future applications in aerospace and ground transportation (Ref 1-3). Combining Mg and Al alloys in the most efficient and effective manner possible is a highly worthwhile research target, but despite the substantial potential for cost reduction and ecological impact, the application of Mg/Al joints remains limited. It is relatively challenging to fabricate Mg and Al alloys using currently available welding methods.

The formation of Mg-Al brittle intermetallic compounds (IMCs) in welds is the primary factor resulting in the poor

Qiong Gao and Kehong Wang, School of Materials Science and Engineering, Nanjing University of Science and Technology, Nanjing 210094, China. Contact e-mails: gqiong88@163.com and wkh1602@126.com.

strength of Mg/Al joints (Ref 4, 5). Many previous research studies have focused on controlling the growth of Mg/Al IMCs by controlling the welding process. For example, Wang et al. proposed laser-arc-adhesive hybrid welding with a Ni interlayer (Ref 6), and found that the harmful effects of Mg/Al IMCs were reduced significantly and that joint properties were improved compared to those without a Ni interlayer. Patel et al. adopted ultrasonic spot welding to combine Mg and Al (Ref 7), and found that an $Mg_{17}Al_{12}$ IMC layer formed at the weld center and that failure occurred between the Al alloy and the intermetallic layer. Dietrich et al. used diffusion welding to create Al and Mg alloys (Ref 8), and found that changing the Al-based solid solution in the interface region influenced the mechanical properties of the joint. Friction stir welding, an innovative welding process, has been investigated in several studies (Ref 9-12); the process results in favorable joint performance due to Mg-Al IMC reduction, but unfortunately, Mg-Al IMCs are not eliminated entirely. Although solid-state welding processes show considerable potential for welding Mg-Al alloys with high strength Mg/Al joints, they are somewhat limited in application due to inflexible manipulation. Gas tungsten arc welding (TIG), a conventional fusion welding process already commonly used in the aerospace and automotive industry, may ameliorate certain disadvantages owing to its low cost and relatively simple operation, potentially solving problems inherent to combining Mg and Al metals.

Liu et al. described two methods for successfully welding Mg and Al: first, improving the welding speed, (i.e., keeping heat input low,) and second, choosing a proper filler metal (Ref 13). Previous studies have used Zn as an alloying material for joining Al and Mg alloy, with mixed results (Ref 14-17). As an alloying element, Zn preferentially reacts with Mg to form Mg-Zn IMCs instead of Mg-Al IMCs, resulting in enhanced mechanical properties of Al/Mg joints. However, based on the Mg-Al-Zn ternary phase diagram, Mg, Al, and Zn can react to form a variety of Mg-Zn IMCs and Mg-Al-Zn IMCs. The type

and distribution of IMCs generated in the weld zone differ when adjusting the Zn addition; and as such, the effects of Zn addition on interfacial microstructure and mechanical properties of Mg/Al joints remain unclear. In this study, 6061 Al alloy and AZ31B Mg alloy were welded by TIG lap welding with Zn foils of varying thicknesses, and the influences of the Zn interlayer on interfacial microstructure and mechanical properties of Mg/Al TIG lapping welding joints, as well as the fracture mechanisms in the joint, were analyzed in detail.

2. Experimental Methods

Sheets of 6061 aluminum and AZ31B magnesium alloys were adopted as base materials in this experiment. (dimensions: 4 mm × 50 mm × 110 mm). The typical chemical compositions of the base metals are provided in Table 1. According to Borrisutthekul et al., the edge-line welding of a lap joint can easily control the thickness of an intermetallic layer to ensure high joint strength (Ref 18). Based on this principle, we attempted to use TIG impenetrable lapping welding which has lower heat input, rather than butt welding. In order to observe the influence of Zn addition on the weld properties, pure Zn foils were added between Mg and Al sheets of thicknesses of 0.1, 0.2, 0.3, 0.4, and 0.5 mm. The experimental configuration is shown in Fig. 1. The Al sheet was placed on the top of the Mg sheet with an overlap distance of 15 mm, and the angle α between the TIG torch and perpendicular line was 15°. Before welding, the oxides and oil on the surface of the sheets and Zn foils were removed by mechanical polishing with acetone. The

welding parameters applied were welding current of 190 A, welding voltage of 17.2 V, and welding speed of 40 cm/min.

After welding, the transverse sections of the welds were polished and etched for microstructural observation. The joint microstructures were observed under a scanning electron microscope (SEM) (FEI Quanta 250F environment scanning electronic telescope) equipped with an energy dispersive x-ray spectrometer (EDS). The elemental distribution and phase constituents of the joints were measured by EDS and x-ray diffraction (XRD) (Bruker D8 x-ray diffractometer), respectively.

Each welded seam was cut into three identical tensile shear specimens 10 mm in width and 50 mm in gauge length. A sketch of the lapping welding tensile shear specimens is shown in Fig. 2. The tensile shear tests were conducted at room temperature at a stretching rate of 1 mm/min. Joint tensile shear strength (TSS) was evaluated according to the average maximum loads and welding areas of the three samples, and the location and characteristics of fractures in the Al-Mg welded joints were analyzed by SEM and XRD, respectively.

3. Results and Discussion

3.1 Effects of Zn Addition on Joint Tensile Shear Strength

To evaluate the effects of Zn thickness on the TIG lapping weld joint strength, TSS testing was conducted in shear mode as shown in Fig. 3. [TSS is equivalent to $1/\sqrt{3}$ of the tensile strength of the same material (Ref 18).] We found that Zn interlayer thickness had a significant influence on Al/Mg joint

Table 1 Chemical compositions (wt.%) of AZ31B and 6061 alloys

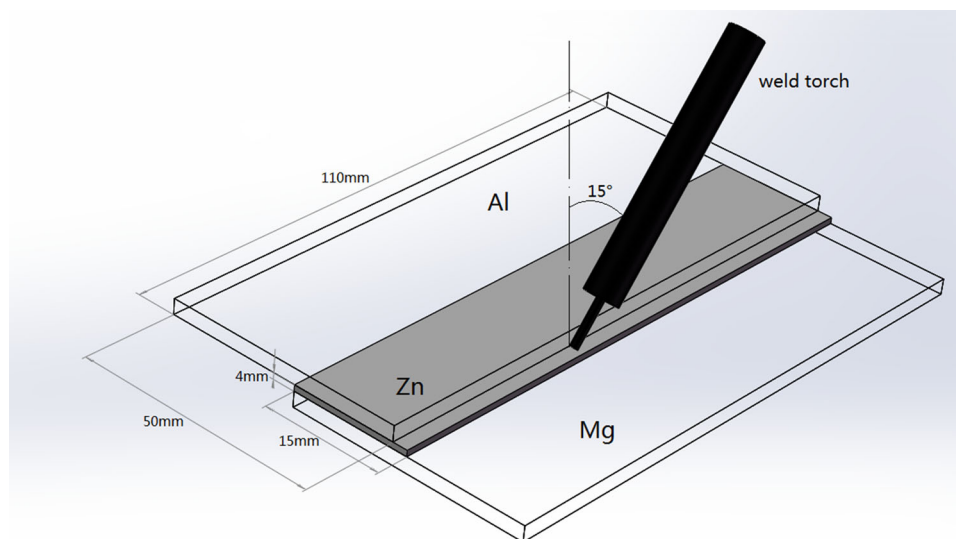| Material	Al	Zn	Mn	Si	Fe	Cu	Ca	Cr	Mg	Other
AZ31B	2.5-3.5	0.6-1.4	0.2	0.1	0.005	0.05	0.04	…	Bal	0.3
6061	Bal	0.250	0.15	0.4-0.8	0.7	0.15-0.4	…	0.04-0.35	0.8-1.2	0.15

Fig. 1 Configuration and dimensions of TIG lapping welding
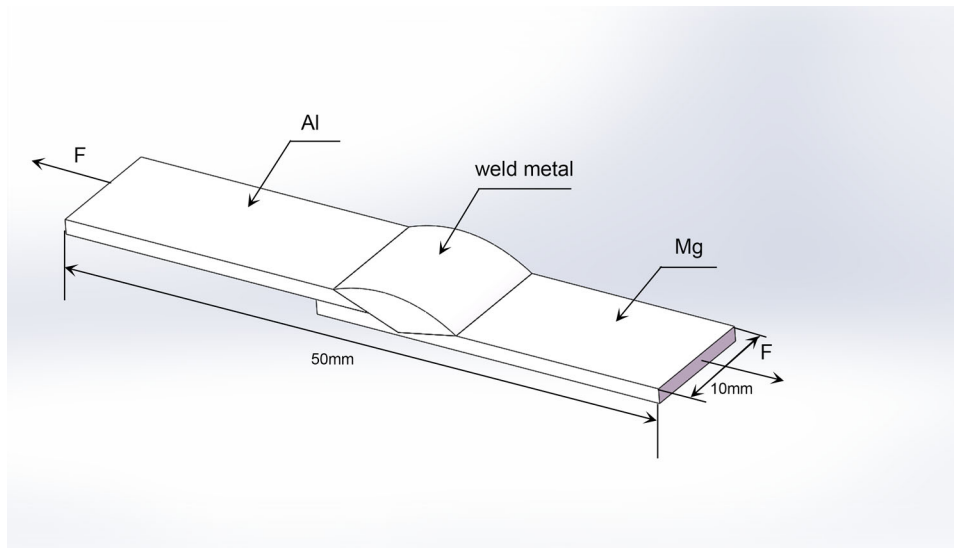
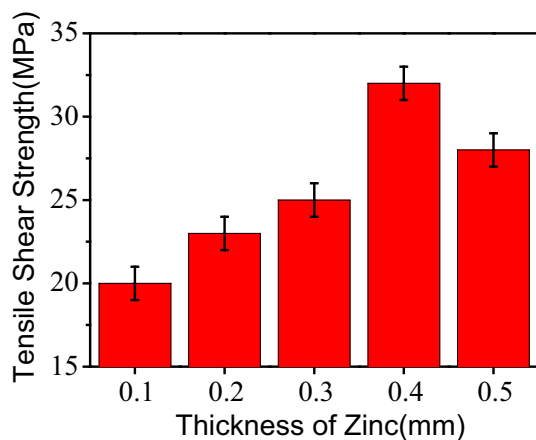**Fig. 2** Sketch of lapping welding tensile shear test specimens (mm)

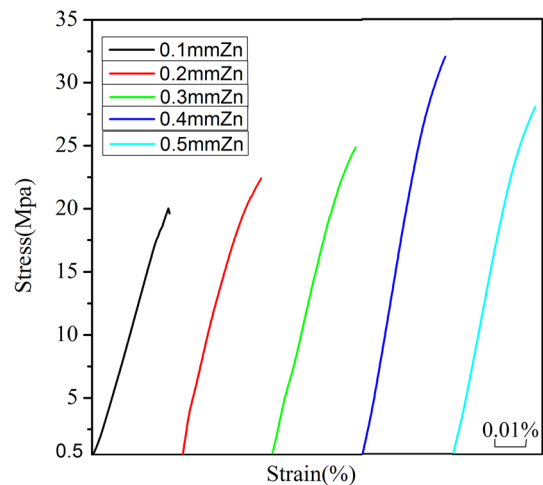**Fig. 3** TSS of TIG lapping welded joints with differing Zn interlayer thicknesses

Fig. 4 Stress-strain curves of TIG lapping welded joints with differing Zn interlayer thicknesses

properties—as Zn interlayer thickness increased, the TSS of the welded joints increased. The highest TSS value was 32 MPa, at 0.4-mm Zn interlayer thickness. When Zn interlayer thickness increased to 0.5 mm, however, the TTS of the welded joint dropped to 28 MPa. The minimum LSS value was 20 MPa, at 0.1-mm Zinc interlayer thickness. The stress-strain curves of TIG lapping welded joints with differing Zn interlayer thicknesses are shown in Fig. 4. We found that there is some plastic deformation before the fracture of all the TIG lap welded joints with differing Zn interlayer thicknesses. It can be concluded that fracture mode of the joints with differing Zn interlayer thicknesses were brittle in nature.

Cross sections of the fractured welds' joints with Zn foils from 0.1 to 0.5 mm in thickness were observed by SEM as shown in Fig. 5. There was a transitional zone (TZ) between the Mg alloy substrate and fusion zone (FZ) and the joints with 0.1-, 0.2-, and 0.3-mm-thick Zn foils were fractured at the TZ near the Mg substrate. The joints with 0.4- or 0.5-mm-thick Zn foil, however, were fractured at the FZ.

The phase constituents of the fracture surfaces of Al/Mg joints were observed by XRD as shown in Fig. 6. The K calculating method was adopted to calculate the content of $Mg_{17}Al_{12}$ and Mg_2Al_3, as shown in Fig. 7. The XRD results indicated that the fracture surfaces of Al/Mg joints with 0.1-, 0.2-, and 0.3-mm-thick Zn interlayers consisted of $Mg_{17}Al_{12}$, Mg_2Al_3 IMCs, and $MgZn_2$ IMCs. When Zn layer thicknesses increased to 0.4 and 0.5 mm, there were very little amounts of Mg-Al IMCs found in the fracture surfaces, suggesting that proper Zn interlayers can prevent the formation of Al-Mg IMCs. Despite the Mg-Al IMCs, there were a large amount of Mg-Zn IMCs continuously distributed in the FZ near the Mg side. In the joint with 0.4-mm-thick Zn foil, the interlayer near the Mg side was composed of Al-based solid solution and $Mg_{32}(AlZn)_{49}$ strengthened phase. Due to excessive Zn content, the XRD result showed that the joint with 0.5-mm-thick Zn foil was composed of new phase $(AlMg_4Zn_{11})$, $Mg_{32}(AlZn)_{49}$, and Al-based solid solution.
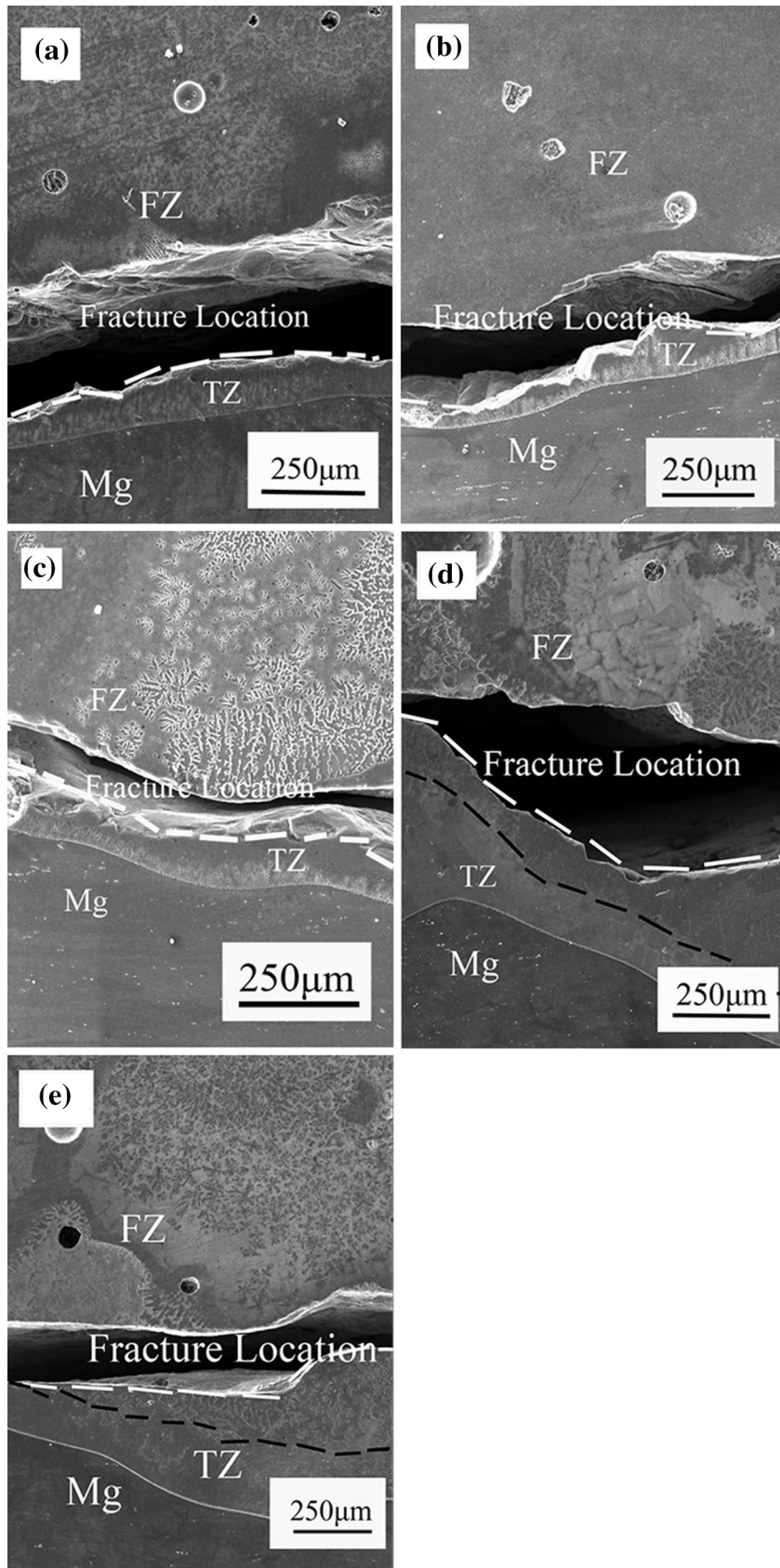
Fig. 5 Fracture locations of joints using Zn foils of different thicknesses added: (a) 0.1-mm Zn foil, (b) 0.2-mm Zn foil, (c) 0.3-mm Zn foil, (d) 0.4-mm Zn foil, (e) 0.5-mm Zn foil
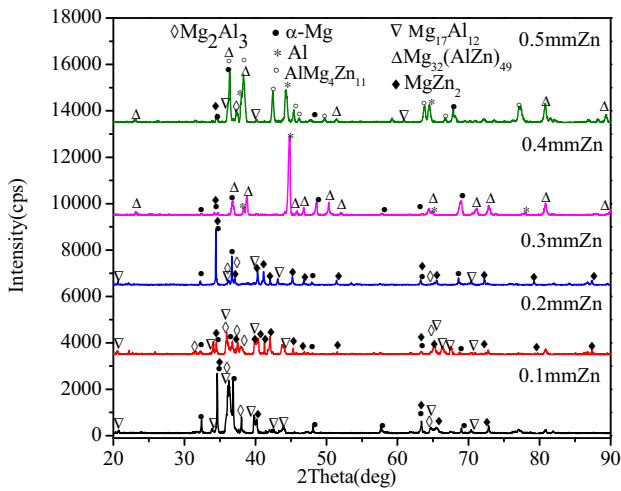
Fig. 6 X-ray diffraction spectra obtained from fracture surfaces of joints with different Zn foil thicknesses
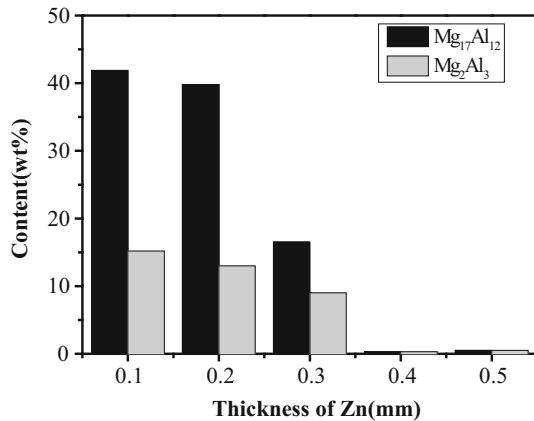

Fig. 7 Mg-Al IMCs contents in joints with different Zn foil thicknesses

The phases in the fracture surfaces of the joints with 0.1-, 0.2-, and 0.3-mm Zn foil are the same as that shown in Fig. 6. The joint with 0.4 mm-thick Zn foil showed the highest TSS, while the joint with 0.1-mm-thick Zn had the lowest. Joint TSS decreased when Zn foil thickness increased to 0.5 mm. We then, accordingly, selectively investigated the microstructures of the weak areas of the three typical joints (0.1-mm-thick Zn foil, 0.4-mm-thick Zn foil, and 0.5-mm-thick Zn foil).

3.2 Microstructures of Weak Area in the Joint

The microstructures of weak area in the three typical joints were observed, and the distributions of major elements (Al, Mg, and Zn) across the fracture location in the joints were tested to determine the cause of fracture. Figure 8 shows the SEM images and corresponding linear SEM-EDS line analysis results of the distributions of major elements (Al, Mg, and Zn) in the joint cross sections with different Zn foil thicknesses. As shown in Fig. 8(a) through (c), a sharp decrease in Mg concentration was observed in the interface between the Mg and interlayer. The same situation is observed in the interface between interlayer and Al, but the elemental diffusion patterns from the Mg side to the weld zone differed notably according to
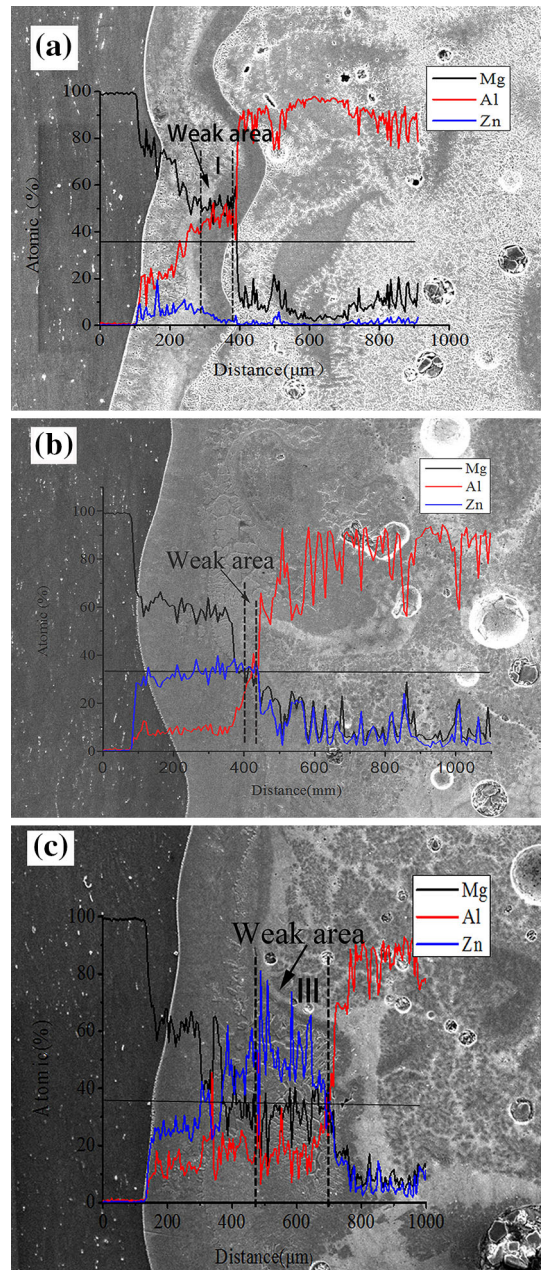

Fig. 8 Linear SEM-EDS analysis of interface layer: (a) 0.1-mm Zn foil, (b) 0.4-mm Zn foil, (c) 0.5-mm Zn foil

different Zn interlayer thicknesses. As Zn foil thickness increased, smaller amounts of Mg and Al elements diffused into the FZ, which impeded the combination of Mg and Al. The weak areas of the joints, shown in Fig. 8(a) through (c), are marked by arrows. Region I in Fig. 8(a) is the weak area of the joints with 0.1-mm-thick Zn foil, where the concentration patterns of Mg and Al are overlapped, which was assumed as a stable step, where Mg-Al IMCs formed preferentially. Figure 8(b) shows the location where the fracture of the joint with 0.4-mm-thick Zn foil occurred along Region II; the stoichiometric ratio of Mg, Al, and Zn in region II was approximately 1:1:1, confirming that Mg-Al-Zn IMCs were generated in this area. Figure 8(c) shows the weak area of the joint with 0.5-mm-thick Zn foil along Region III, which was rich with Zn element. To further investigate the failure mechanism of the joints, the

Table 2   EDS results of various points for three typical joints

Element (at.%)	Point						
	1	2	3	4	5	6	7
Mg	39.20	60.6	37.16	13.26	11.41	28.04	38.23
Al	53.08	33.07	28.68	69.38	69.22	9.89	17.15
Zn	7.72	6.24	34.16	17.36	19.37	62.07	44.62
Possible Phases	Mg_2Al_3	$Mg_{17}Al_{12}$	$Mg_{32}(Al,Zn)_{49}$	Al solid solution, $MgZn_2$	Al solid solution, $MgZn_2$	$AlMg_4Zn_{11}$	Mg solid solution, $MgZn_2$
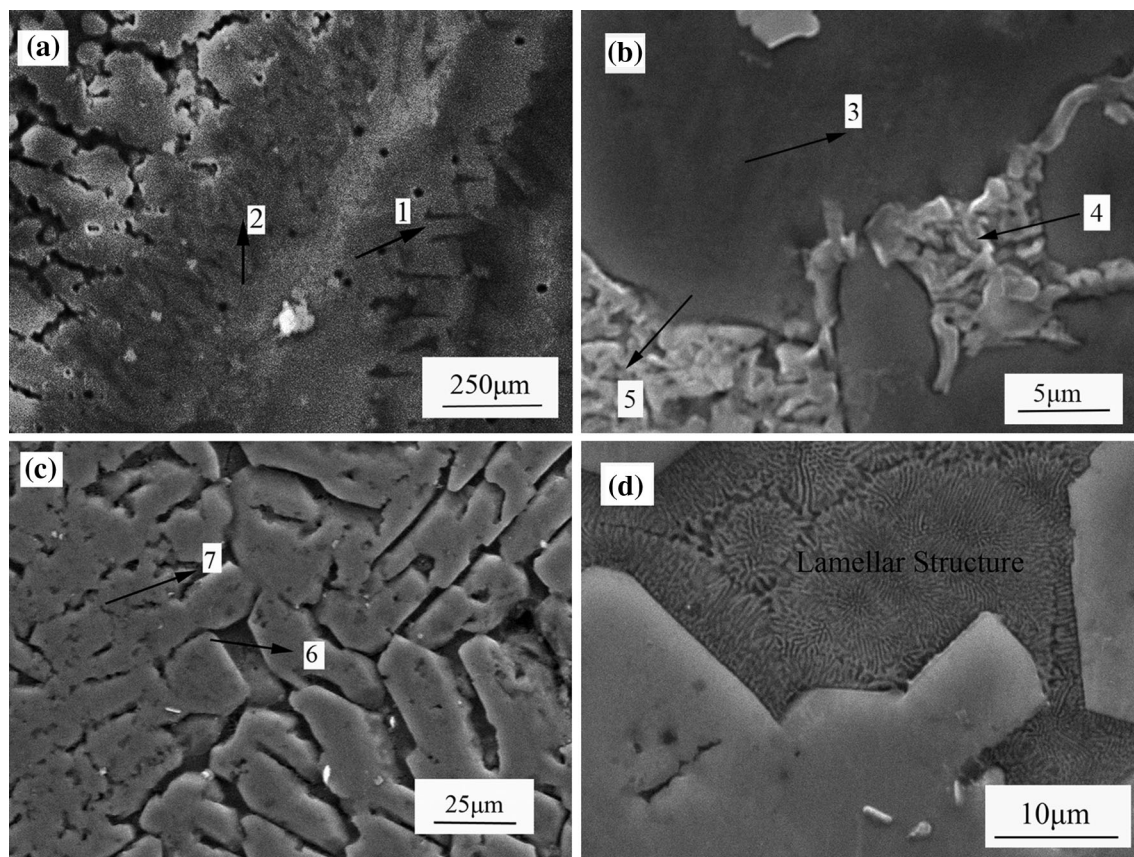
Fig. 9 Microstructures in weak parts of joints with different Zn foils: (a) 0.1-mm Zn foil, (b) 0.4-mm Zn foil, (c) 0.5-mm Zn foil, (d) magnification of Point 7

microstructures of the weak areas of the joints were observed by SEM as shown in Fig. 9(a) through (d).

The chemical compositional analysis results from Position 1 to Position 6, which were used to investigate the phase compositions of the weak parts of the sample weld seams by EDS, are presented in Table 2. Figure 9(a) shows the microstructures in the weak areas of the joint with 0.1-mm-thick Zn foil. Point 1, as shown in Fig. 9(a), contained 39.20 at.% Mg, 53.08 at.% Al, and 7.72 at.% Zn; i.e., atomic ratio of Mg to Al of nearly 2:3, suggesting the presence of Mg_2Al_3 IMCs. Point 2 contained 69.6 at.% Mg, 33.07 at.% Al, and 6.24 at.% Zn, with atomic ratio of Mg and Al at nearly 2:1, suggesting that this area contained $Mg_{17}Al_{12}$. According to EDS and SEM results, the phases in the weak areas of the joint were Mg_2Al_3 and $Mg_{17}Al_{12}$, i.e., hard and brittle material, so the fracture in this location occurred due to the formation of Mg-Al IMCs.

The microstructures shown in Fig. 9(b) are the weak areas of the joint with 0.4-mm-thick Zn foil, which was mainly composed of lamellar microstructure (Point 5 and Point 4) and dark phase (Point 3). The chemical composition in Point 3 was 37.16 at.% Mg, 28.68 at.% Al, and 34.16 at.% Zn; the atomic ratio of Al, Mg, and Zn was nearly 1:1:1. According to the established Mg-Al-Zn ternary phase diagram and EDS results (Ref 19), this represents an Mg-Al-Zn phase—previous research has shown (Ref 20, 21) that this phase is composed of $Mg_{32}(Al,Zn)_{49}$ IMCs. The distribution of $Mg_{32}(Al,Zn)_{49}$ IMCs are continuous, which leads to low ductility and crack origins (i.e., the preferred fracture path.) Point 5 and Point 4 showed rod-like structures; the bending behavior at Point 5 demonstrated very favorable toughness in the material, as there was no fracture even after 90° bending. Similar results were reported by Liu (Ref 22), who conducted TEM tests to confirm that an experimental rod-like structure was composed of $MgZn_2$

and Al solid solution. In our experiment, a dark phase (Point 3) precipitated in the Al solid solution; because the Al solid solution had excellent plasticity, it ameliorated the stress concentration caused by IMCs, improving the TSS of the material. Similar phenomena were observed by Liu et al. (Ref 16), in fact. In addition, the XRD results shown in Fig. 6 confirmed the existence of $Mg_{32}(Al,Zn)_{49}$ and $MgZn_2$ IMCs.

Figure 9(c) shows the microstructure of the weak area of the joint with 0.5-mm-thick Zn foil. Point 6 in Fig. 9(c) is composed of continuous columnar grains, and the dark phase in Point 7 is lamellar eutectic structure as shown in Fig. 9(d). Columnar grains dispersedly embedded in the lamellar eutectic structure. Point 6 contained 28.04% Mg, 9.89 at.% Al, and 62.07 at.% Zn, suggesting that this location was a Zn-rich zone that may have contained an Mg-Al-Zn IMC. The atomic ratio of Al, Mg, and Zn was nearly 4:1:7. According to the Mg-Al-Zn ternary phase diagram, there was an $AlMg_4Zn_{11}$ phase in Point 6, and the lamellar eutectic structure in Point 7 was composed of Mg solid solution and $MgZn_2$. Excessive Zn foil addition caused Zn-rich zones to form, as well as Zn-rich Mg-Al-Zn IMCs, which then damaged the properties of the joint.

In short, a thin Zn interlayer alone does not sufficiently reduce Mg-Al IMCs. In the joint with 0.1-mm-thick Zn foil, IMCs $Mg_{17}Al_{12}$ and Mg_2Al_3 were predominant these hard and brittle IMCs impeded the material's ductility during tensile shear testing. Thicker Zn interlayers prevented the Al and Mg from mixing appropriately, impeding the successful formation of Mg-Al IMCs; these alloys were composed mainly of Mg-Zn IMCs and Mg-Al-Zn IMCs. Fractures occurred at any location where IMCs were continuously distributed. In the joint with 0.4-mm-thick Zn foil, a large number of Al solid solutions precipitated in the IMCs and improved the microstructure, resulting in improved TSS in the joint.

3.3 Joint Fracture Surfaces

The fracture surfaces of three typical joints with 0.1-, 0.4-, and 0.5-mm-thick Zn foils were observed as shown in Fig. 10. Figure 10(a) is the fracture surface of the Al/Mg joint with a 0.1-mm-thick Zn interlayer, where the fracture surface on the Mg alloy side was flat and consisted of air holes and cleavage steps, demonstrating that the fracture mode of Al/Mg joints with 0.1-mm-thick Zn interlayer is one of brittle with no plastic deformation prior to fracture. Dimple-like and quasi-cleavage-like fracture characteristics, as shown in Fig. 10(b) to (c), appeared in the fracture of the Al-Mg joint with 0.4- and 0.5-mm-thick Zn interlayers. The quasi-cleavage fracture mode, as characterized by several tearing ribs and dimples in the cleavage plane, indicated that local plastic deformation occurred before fracture. Basically, higher Zn content improved the microstructure of the fracture zone and improved the TSS of the joint.

3.4 Discussion

We observed substantial improvements in TSS and Al/Mg joint microstructures after adding Zn foil to the sample alloys. As commonly accepted, Mg-Al IMCs are very hard and brittle, so when a large number of Mg-Al IMCs exist in the interlayer of the joints, they act preferentially as the source of microcracks and degrade overall joint properties. Of course, then, a large number of continuous Mg-Al IMCs are undesirable. XRD and EDS results revealed that as Zn interlayer thickness increased from 0.1 to 0.3 mm, the Al-Mg IMCs gradually reduced, while Mg-Zn IMCs ($MgZn_2$) formed at the interface of the joints. The
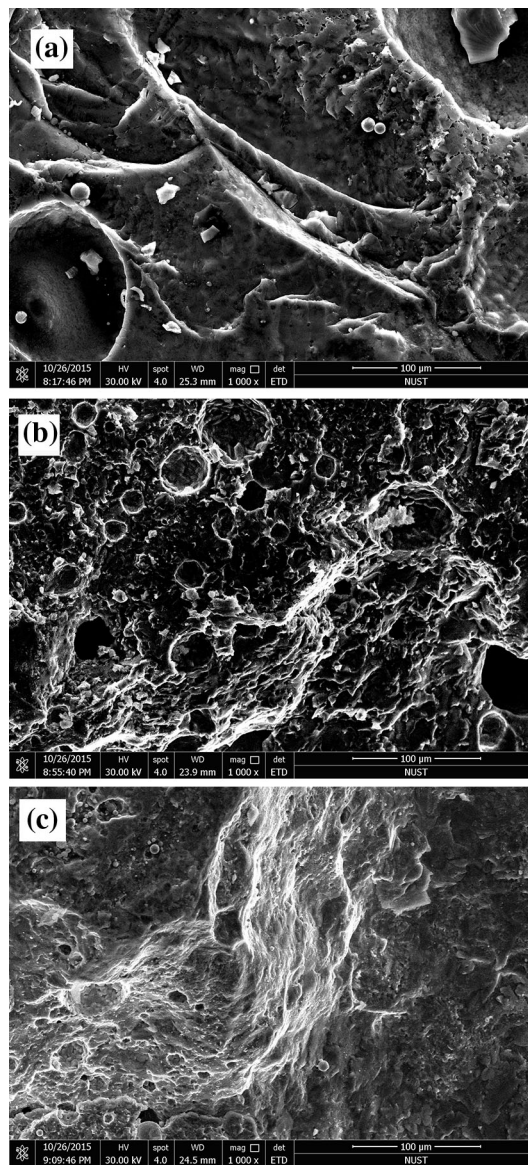
Fig. 10 (a) Fracture surface morphology of Al/Mg joints with 0.1-mm-thick Zn interlayer at Mg side, (b) fracture surface morphology of Al/Mg joints with 0.4-mm-thick Zn interlayer at Mg side, (c) fracture surface morphology of Al/Mg joints with 0.5-mm-thick Zn interlayer at Mg side

Zn interlayer acts as a barrier preventing Mg and Al from diffusing into the FZ. Based on thermodynamic theory, Mg preferentially reacts with Zn resulting in Mg-Zn IMCs instead of Mg-Al IMCs, effectively reducing the amount of Mg-Al IMCs in the alloy. The microstructure of the joint interlayer was improved after adding Zn foil between the Mg and Al substrates, and the TSS of the joints also improved along with the increasing Zn foil thickness.

When the thickness of the Zn layer increased to 0.4 or 0.5 mm, however, bare Al-Mg IMCs resulted (Fig. 6 and 9). The fracture of the joint with 0.4-mm-thick Zn foil was located at the FZ. According to our analysis of weak joint areas ("Microstructures of Weak Area in the Joint" section), the microstructure was composed of Al-based solid solution and $Mg_{32}(AlZn)_{49}$. The thermal stability of the ternary $Mg_{32}(AlZn)_{49}$ phase was better than the binary $Mg_{17}Al_{12}$ and

Mg_2Al_3 phases. A large amount of Al solid solutions precipitated in IMCs eliminate the stress concentration of the crack tip and hinder crack propagation, so improving the TTS of the joint by improving the microstructures in the joint. At Zn foil thickness of 0.5 mm, however, we found that the TTS of the joint decreased. In other words, excessive addition of Zn foil causes partial Zn-rich zones to form, as shown in Fig. 8(c). The partial Zn-rich zones are composed of IMCs ($AlMg_4Zn_{11}$, $Mg_{32}[AlZn]_{49}$) and Al solid solution. When the joint bears tension stress, the continuous distribution of IMCs tends to produce cracks and deteriorate the properties of the joint.

4. Conclusions

In this study, the effects of different thicknesses of Zn foil on the microstructure and mechanical properties of Mg/Al joints welded by TIG lapping welding were analyzed in detail. The most important conclusions of this study can be summarized as follows:

1. AZ31B Magnesium alloy and 6061 aluminum alloy were successfully welded by TIG lapping welding with differing thicknesses of Zn foil; Zn foil thickness significantly influenced the Al/Mg joint properties and microstructure. High Zn interlayer thickness (0.4 mm) improved mechanical properties, but excessive Zn thickness (0.5 mm) degraded mechanical properties. We assert that 0.4-mm-thick Zn foil addition is appropriate for TIG lapping welding of AZ31B magnesium to 6061 aluminum alloy.
2. The addition of Zn foil with 0.4-mm thickness also refined the microstructure of the Al/Mg joint, effectively avoiding the formation of Mg/Al IMCs. The fracture was located at the FZ, composed of Al-based solid solution and $Mg_{32}(AlZn)_{49}$. Al solid solution was precipitated in the IMCs to improve the microstructure, thus improving the TSS of the joint.
3. Adding Zn foil with 0.4-mm thickness also changed the fracture mode of the material. The fracture mode of Al/Mg joints with a 0.1-mm-thick Zn interlayer was one of brittle, with no plastic deformation prior to fracture; the fracture modes of Al/Mg joints with 0.4- and 0.5-mm-thick Zn interlayers were of quasi-cleavage, characterized by several tearing ribs and dimple-like structures in the cleavage plane, indicating that local plastic deformation occurred before fracture.

References

1. E. Schubert, M. Klassen, I. Zerner, C. Walz, and G. Sepold, Light-Weight Structures Produced by Laser Beam Joining for Future Applications in Automobile and Aerospace Industry, *J. Mater. Proc. Technol.*, 2001, **115**, p 2–8
2. W.S. Miller, L. Zhuang, J. Bottema, A.J. Wittebrood, P. De Smet, A. Haszler, and A. Vieregge, Recent Development in Aluminum Alloys for the Automotive Industry, *Mater. Sci. Eng. A.*, 2000, **280**, p 37–49
3. B.L. Mordike and T. Ebert, Magnesium: Properties-Applications-Potential, *Mater. Sci. Eng. A.*, 2001, **302**, p 37–45
4. R. Cao, B.F. Wen, J.H. Chen, and P.-C. Wang, Cold Metal Transfer Joining of Magnesium AZ31B-to-Aluminum A6061-T6, *Mater. Sci. Eng. A.*, 2013, **560**, p 256–266
5. D.-H. Choi, B.-W. Ahn, C.-Y. Lee, Y.-M. Yeon, K. Song, and S.-B. Jung, Formation of Intermetallic Compounds in Al and Mg Alloy Interface During Friction Stir Spot Welding, *Intermetallics.*, 2011, **19**, p 125–130
6. H. Wang, L. Liu, and F. Liu, The Characterization Investigation of Laser-Arc-Adhesive Hybrid Welding of Mg to Al Joint Using Ni Interlayer, *Mater. Des.*, 2013, **50**, p 463–466
7. V.K. Patel, S.D. Bhole, and D.L. Chen, Microstructure and Mechanical Properties of Dissimilar Welded Mg-Al Joints by Ultrasonic Spot Welding Technique, *Sci. Technol. Weld. Jt.*, 2012, **17**, p 202–206
8. D. Dietrich, D. Nickel, M. Krause, T. Lampke, M.P. Coleman, and V. Randle, Formation of Intermetallic Phases Diffusion-Welded Joints of Aluminum and Magnesium Alloys, *J. Mater. Sci.*, 2011, **46**, p 357–364
9. Y. Sato, S. Park, M. Michiuchi, and H. Kokawa, Constitutional Liquation During Dissimilar Friction Sir Welding of Al and Mg Alloys, *Scr. Mater.*, 2004, **50**, p 1233–1236
10. A. Kostka, R.S. Coelho, J. dos Santos, and A.R. Pyzalla, Microstructure of Friction Stir Welding of Aluminum Alloy to Magnesium Alloy, *Scr. Mater.*, 2009, **60**, p 953–956
11. Y.J. Kwon, I. Shigematsu, and N. Saito, Dissimilar Friction Stir Welding Between Magnesium and Aluminum Alloys, *Mater. Lett.*, 2008, **62**, p 3827–3829
12. U. Suhuddin, V. Fischer, F. Kroeff, and J.F. dos Santos, Microstructure and Mechanical Properties of Friction Spot Welds of Dissimilar AA5754 Al and AZ31 Mg Alloys, *Mater. Sci. Eng. A.*, 2014, **590**, p 384–389
13. L. Liu, X. Liu, and S. Liu, Microstructure of Laser-TIG Hybrid Welds of Dissimilar Mg Alloy and Al Alloy with Ce as Interlayer, *Scr. Mater.*, 2006, **55**, p 383–386
14. H.T. Zhang and J.Q. Song, Microstructural Evolution of Aluminum/Magnesium Lap Joints Welded Using MIG Process with Zinc Foil as an interLayer, *Mater. Lett.*, 2011, **65**, p 3292–3294
15. L.M. Zhao and Z.D. Zhang, Effect of Zn Alloy Interlayer on Interface Microstructure and Strength of Diffusion-Bonded Mg-Al Joint, *Scr. Mater.*, 2008, **58**, p 283–286
16. F. Liu, Z. Zhang, and L. Liu, Microstructure Evolution of Al/Mg Butt Joints Welded by Gas Tungsten Arc with Zn Filler Metal, *Mater. Charact.*, 2012, **69**, p 84–89
17. F. Liu, H. Wang, and L. Liu, Characterization of Mg/Al Butt Joints Welded by Gas Tungsten Arc Filling with Zn-29.5Al-0.5Ti Filler Metal, *Mater. Charact.*, 2014, **90**, p 1–6
18. R. Borrisutthekul, Y. Miyashita, and Y. Mutoh, Dissimilar Material Laser Welding Between Magnesium Alloy ZA31B and Aluminum Alloy A5052-O, *Sci. Technol. Adv. Mater.*, 2005, **6**, p 199–204
19. V. Pierre, P. Alan, and H. Okamoto, *Handbook of Ternary Alloy Phase Diagrams*, ASM International, Ohio, 1995
20. M. Ohno, R. Mirkovic, and R. Schmid-Fetzer, Phase Equilibria and Solidification of Mg-Rich Mg-Al-Zn Alloys, *Mater. Sci. Eng.*, 2006, **421**, p 328–337
21. M. Ohno, R. Mirkovic, A. Pish et al., Liquidus and Solidus Temperatures of Mg-Rich Mg-Al-Mn-Zn Alloys, *Acta Mater.*, 2006, **54**, p 3883–3891
22. F. Liu, H. Wang, and L. Liu, Characterization of Mg/Al Butt Joints Welded by Gas Tungsten Arc Filling with Zn-29.5Al-0.5Ti Filler Metal, *Mater. Charact.*, 2014, **90**, p 1–6